Proc. Instn Civ. Engrs, Part 2, 1991, **91**, Sept., 561–576
PAPER 9753 MARITIME BOARD

Effects of depth, bed slope and scaling on tidal currents and exchange in a laboratory model harbour

R. A. FALCONER, BSc(Eng), MSCE, PhD, DIC, MICE, FIWEM, MASCE*

YU GUOPING, MSc, PhD†

Details are given of the measured depth-averaged velocity distributions and exchange coefficients for a physical model of a square harbour with a single asymmetric entrance. The model was based on typical harbour shapes in the USA and the UK; the tidal conditions were typical of those in the UK. For these tests, emphasis was placed on determining the influence of the mean depth, bed slope and vertical scale distortion on the tidal current structure at mean water level, for both ebb and flood tides, and on the tidal exchange characteristics at the end of four tidal cycles. Velocity distributions were measured along the centre-line axes of the model, with the axes intersecting at the harbour centre. For the exchange characteristics, gross tidal exchange coefficients were determined from local exchange values at 25 equidistant sites within the model harbour, for both horizontal and uniformly sloping beds. The results showed that the tidal exchange coefficient decreased with increasing mean depths and increased for increasing bed slopes. However, in connection with the effects of scaling, the results generally suggested that increased distortion appeared to lead to increased exchange coefficients. The comprehensive data set also provided valuable verification data for numerical hydrodynamic water quality models.

Notation

A	plan cross-sectional area of harbour
C	de Chezy roughness coefficient
C_e	eddy viscosity coefficient
C_f	bed friction coefficient
C_i	mean model concentration after i tides
C_0	mean initial model concentration
D	total depth of water column
$D_{xx}, D_{xy}, D_{yx}, D_{yy}$	depth mean dispersion–diffusion coefficients
E	average per cycle exchange coefficient
E_j	local exchange at site j
$\bar{E}$	mean local exchange coefficient
F_r	Froude number
g	gravitational acceleration
h	depth of water column below still water level
H	tidal range
i	number of tidal cycles
j	site location in model harbour

Written discussion closes 15 November 1991; for further details see p. ii.

* Professor of Water Engineering, Department of Civil Engineering, University of Bradford.
† Department of Environmental Engineering, Tongji University, Shanghai, People's Republic of China.

k_ℓ	longitudinal dispersion coefficient
k_t	turbulent diffusion coefficient
L	horizontal length scale
R_b	bed-generated turbulence scaling parameter
R_d	dispersion–diffusion scaling parameter
t	time
T	tidal period
U_0	spatially mean entrance velocity
U_*	shear velocity
U, V	depth mean velocity components in x, y directions
$\|U\|$	depth mean fluid speed
W	entrance width
x, y	horizontal coordinate directions
Z	vertical length scale
β	momentum correction coefficient
ε	depth mean eddy viscosity
ζ	water surface elevation above still water level
λ	bed friction scaling parameter
ρ	fluid density
ϕ	depth mean solute concentration
τ_{bx}	bed shear stress component in x direction
ω	depth-averaged vorticity

Introduction

The Paper gives details of the second stage of a long-term research programme to investigate the tidal current structure and tidal exchange characteristics for a range of idealized rectangular harbours with varying geometric, kinematic and hydrodynamic conditions. In the first series of tests,[1,2] tidal currents were measured for flat bottomed model harbours, with the main aims being to investigate systematically the effects of scale distortion in physical hydraulic tidal models, and to provide a detailed velocity data set against which two-dimensional numerical models of tidal flows in small harbours could be verified. In the current study, this work was extended to include dye tracer studies leading to evaluation of tidal exchange coefficients, and in particular depth–mean velocity distributions and gross concentration measurements for varying mean depths, bed slopes and geometric scales. This subsequent data set also provides further laboratory results against which numerical model predictions can be compared, particularly when the numerical model is run to simulate the laboratory model both in dimensions and time.

2. The main reason for wishing to study the effects of scaling further in this study was derived from the results of earlier investigations by Falconer and Mardapitta-Hadjipandeli[3,4] in which numerical model simulations of the velocity and solute concentration distributions showed some serious discrepancies, particularly on the ebb tide, between the predicted results at laboratory and prototype scales for tide-induced circulation in a square harbour. The scaling ratios used in the earlier studies were 1 : 500 horizontally and 1 : 50 vertically, with dimensions and tide conditions being similar—but not identical—to those used in the current study.

3. This disparity between the numerical model results at laboratory and prototype scales was assumed to be partly attributed to the scaling, based on an analysis of the model-to-prototype scaling ratios obtained from non-dimensionalizing the depth integrated momentum and advective-diffusion equations.

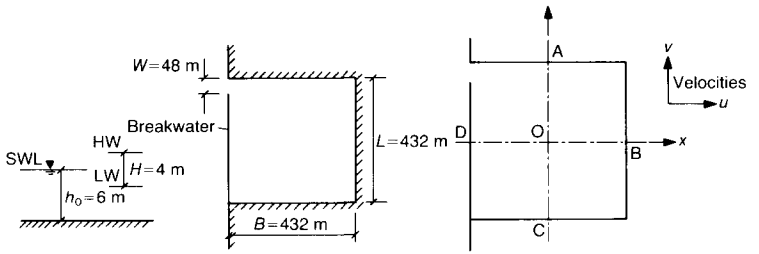

Fig. 1. Illustration of harbour dimensions and coordinate system

4. As for the initial study,[1] the physical laboratory model was stimulated by the continuing worldwide demand for harbours and marinas with the idealized prototype harbour having a square plan cross-sectional area of 0·187 km^2 (i.e. 432 m × 432 m), a single asymmetric entrance width of 48 m, a standard mean still water depth of 6 m, and repetitive semi-diurnal tides of range 4 m and period 12·42 h. The dimensions and single asymmetric entrance configuration are representative of small harbours and marinas in the USA[5] and larger marinas in the UK, with the mean water depth and tidal range being representative of spring tide conditions around much of the United Kingdom coastline. An illustration of the prototype model is shown in Fig. 1, with the corresponding physical model being designed using a conventional Froude law scaling relationship, and the scale ratios are given in Table 1. The tests involving variations in the mean depth included prototype depths of 4, 5, 6, 7, 8 and 9 m and variations in the horizontal scale of 1 : 400 and 1 : 200, respectively.

5. As for previous studies, the dimensions and geometric features of the laboratory basin were governed by the objective of fitting several different grid sizes perfectly into the square harbour shape and across the asymmetric entrance. Numerical model studies of the laboratory basin were undertaken using three different grid sizes, including 12, 6 and 4 cm.

Experimental arrangement

6. The model harbours (at 1 : 400 and 1 : 200 horizontal scales and with dimensions as given in Table 2) were constructed of plywood and consisted of four vertical sidewalls and a flat bed, which was either horizontal or sloped for the corresponding test conditions. The model was positioned at one end of a

Table 1. Scale ratios considered for laboratory tests

Horizontal scale	Vertical scale	Distortion ratio	Model period : s
1 : 400	1 : 33·3	12 : 1	646
1 : 400	1 : 40	10 : 1	708
1 : 400	1 : 64	6·25 : 1	894
1 : 200	1 : 33·3	6 : 1	1292
1 : 200	1 : 40	5 : 1	1416
1 : 200	1 : 64	3·125 : 1	1788

Table 2. Model harbour dimensions

Model dimension		1 : 400 scale	1 : 200 scale
Length		1·08 m	2·16 m
Entance width		120 mm	240 mm
Mean depth	1 : 64	94 mm	94 mm
	1 : 40	150 mm	150 mm
	1 : 33	180 mm	180 mm
Tidal periods	1 : 64	894 s	1788 s
	1 : 40	708 s	1416 s
	1 : 33	646 s	1292 s

5·32 m × 3·8 m × 0·62 m deep PVC tidal tank, with the harbour bed being raised above the floor of the tidal tank to give the correct still water level working depth in the model (Fig. 2).

7. Constant amplitude and constant period model tides were reproduced in the tidal tank by means of a vertically oscillating weir, located just inside the tidal tank and opposite the model harbour. Although the design permitted the generation of varying non-sinusoidal tides, only repetitive sinusoidal tides were considered in the tests described herein. Adjacent and parallel to the weir was a

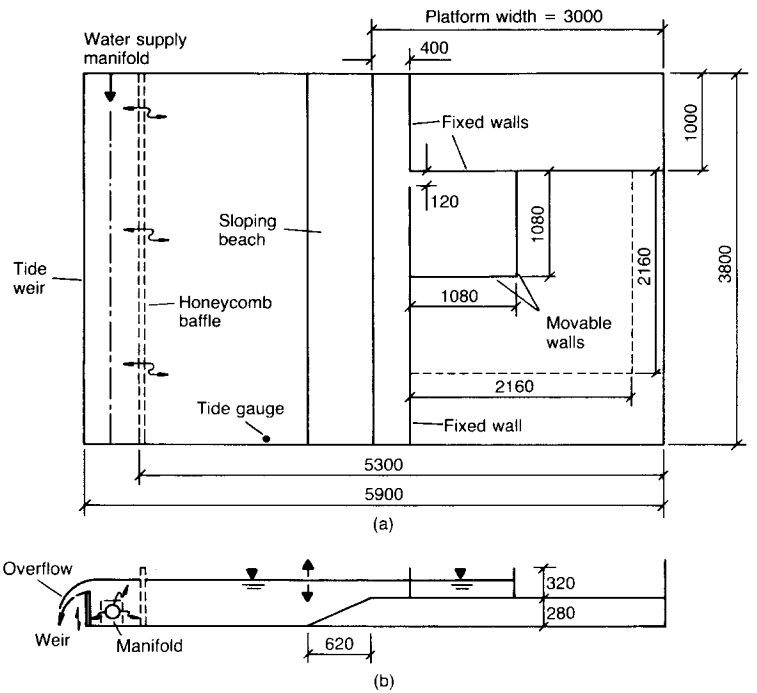

Fig. 2. Illustration of laboratory tidal basin and harbour configuration: (a) tide tank-plan; (b) section through harbour (dimensions in mm)

constant rate water supply diffuser which delivered just sufficient water upstream of the weir to produce a small overflow over the weir. The water surface elevation was measured in the tank using a Churchill conductivity water level recorder and a Scan Technologies ultrasonic level recorder. The actual measured tides were found to be close to sinusoidal in form, and the model tides lagged the weir motion by approximately 6° at the harbour entrance.

8. The velocities in the model harbour were measured using two different techniques. For the 1 : 400 model, weighted plastic floats were used, penetrating at least 80% of the water column to follow the local depth-averaged tidal current. The floats were tracked visually.[2] Measurements were taken over a period of 1 s before and after the mean water level, for the flood and ebb tides, with the floats inserted just upstream of a pre-determined coordinate along the intersecting axes AOC and BOD (Fig. 1). The velocities were determined for each repetitive flood and ebb tide until sufficient data were obtained to define the velocity profiles along the harbour axes.

9. For the 1 : 200 model with plan cross-sectional dimensions of 2·16 m × 2·16 m, the basin was too large ideally to track floats—other than near the sides—and a series 3 two component electromagnetic current meter was used. The current meter was located at the theoretical location of the depth mean velocity for an assumed logarithmic vertical velocity profile (i.e. 0·4 × D above the bed, where D is the water column depth), with the velocity meter located at approximately 67 mm increments along the intersecting axes. As before, measurements were taken within only ±10 s of the mean water level.

Analysis procedure

10. All measured velocities were normalized by dividing them by a reference velocity U_0. This reference velocity was obtained by applying a simplified form of the one-dimensional continuity equation, wherein the discharge across the harbour entrance was equated to the volume change per unit time within the harbour; that is

$$U_0 = \frac{A \dfrac{d(h + \zeta)}{dt}}{WD} \tag{1}$$

where A is the plan cross-sectional area of harbour, W is the entrance width, h is the depth of water column below mean water level, ζ is the water elevation above mean water level and D is the total depth of water column. With all velocities being measured at (or near to) mean water level, this equation is reduced to

$$U_0 = \frac{\pi AH}{TWh} \tag{2}$$

where H is the tidal range and T is the tidal period. The corresponding reference velocities for the vertical scale ratios of 1 : 33, 1 : 40 and 1 : 64 were 31·51, 28·75 and 22·71 mm/s, respectively.

11. In determining the exchange characteristics, the vertically oscillating weir was first set at low tide. The harbour entrance was then temporarily sealed and a standard volume (25–60 cc for the smaller harbour) of rhodamine B was thoroughly mixed with the enclosed harbour volume. After the turbulence caused by the mixing had decayed, the end of an inflow tube to a continuous flow-through

Turner fluorimeter was submerged within the water column at 25 fixed points within the harbour, and the initial concentration was then determined at all these points. The spatially average initial concentration (C_0) of rhodamine within the harbour was then determined. The temporary barrier across the harbour entrance was removed and the tidal generator switched on and run for four complete tides. At the end of the fourth tidal cycle the generator was stopped and the temporary barrier was simultaneously replaced. The harbour volume was again thoroughly mixed and the average final concentration of enclosed rhodamine was determined as before.

12. From the initial and final concentration measurements, it was possible to determine the average per tidal cycle exchange coefficient for each harbour scaling ratio and mean depth. The observed exchange coefficient is defined as that fraction of water in the basin at high water slack which is removed, or flushed out, from the basin and replaced by ambient water during the cycle ending at the next high water slack.[6] In equation form, it can be expressed as

$$E = 1 - (C_i/C_0)^{1/i} \tag{3}$$

where E is the average per cycle exchange coefficient, C_0 is the initial spatially averaged concentration and C_i is the final spatially averaged concentration after i tidal cycles.

13. For the larger model harbour (size 2·16 m × 2·16 m), in addition to evaluating the gross tidal exchange coefficient, the local exchange coefficient was also evaluated at 25 equidistant sites. For this purpose, continuous flow-through measurements were taken at the 25 sites, at the start of the test and at low tide at the end of the consecutive fourth tide. The local exchange coefficient at site j was evaluated as for the gross exchange given in equation (3), with the gross exchange coefficient also being evaluated from the mean local exchange coefficient; that is

$$\bar{E} = \frac{\sum_{j=1}^{25} E_j}{25} \tag{4}$$

where E_j is the local exchange coefficient at site j and $\bar{E}$ is the mean local exchange coefficient.

Theoretical analysis

14. In predicting the effects of scaling on the bottom friction, turbulence and dispersion–diffusion processes relating to tidal exchange in harbours, it is first convenient to express the depth-integrated x-direction momentum equation excluding rotational effects in the form[4]

$$\frac{\partial UD}{\partial t} + \beta\left[\frac{\partial U^2 D}{\partial x} + \frac{\partial UVD}{\partial y}\right] + gD\frac{\partial \zeta}{\partial x} + \frac{\tau_{bx}}{\rho} - \left[\frac{\partial}{\partial x} 2\varepsilon D \frac{\partial U}{\partial x} + \frac{\partial}{\partial y} \varepsilon D\left(\frac{\partial U}{\partial y} + \frac{\partial V}{\partial x}\right)\right] = 0 \tag{5}$$

where U and V are the depth-averaged velocity components in the x and y coordinate directions, β is the momentum correction factor for non-uniform velocity profile, g is the acceleration due to gravity, τ_{bx} is the bed shear stress component in the x direction, ρ is the fluid density and ε is the depth mean eddy viscosity. The bed shear stress can be expressed in the form of a quadratic friction

law, giving

$$\tau_{bx} = \rho C_f U |U| \tag{6}$$

where C_f is the resistance coefficient and $|U|$ is the depth-averaged fluid speed. Assuming bed-generated turbulence is much greater than free shear layer turbulence, the eddy viscosity can be simplified to give

$$\varepsilon = C_e U_* D = C_e \sqrt{(g)} |U| DC^{-1} \tag{7}$$

where C_e is the eddy viscosity coefficient, U_* is the shear velocity and C is the de Chezy roughness coefficient.

15. Likewise, the advective diffusion equation can be written as

$$\frac{\partial \phi D}{\partial t} + \frac{\partial \phi UD}{\partial x} + \frac{\partial \phi VD}{\partial y} = \frac{\partial}{\partial x}\left[DD_{xx}\frac{\partial \phi}{\partial x} + DD_{xy}\frac{\partial \phi}{\partial y}\right] + \frac{\partial}{\partial y}\left[DD_{yx}\frac{\partial \phi}{\partial x} + DD_{yy}\frac{\partial \phi}{\partial y}\right] \tag{8}$$

where ϕ is the depth-averaged solute concentration and D_{xx}, D_{xy}, D_{yx}, and D_{yy} are the depth-averaged longitudinal dispersion and turbulent diffusion tensor coefficients. As for the eddy viscosity, the dispersion–diffusion coefficients are of a similar form, giving for the x direction

$$\left.\begin{aligned} D_{xx} &= \frac{C_f(k_\ell U^2 + k_t V^2)}{|U|} \\ D_{xy} &= \frac{C_f(k_\ell - k_t)UV}{|U|} \end{aligned}\right\} \tag{9}$$

where k_ℓ is the depth-averaged longitudinal dispersion coefficient and k_t is the depth-averaged lateral diffusion coefficient.

16. The corresponding non-dimensionalized forms of equations (5) and (8) are, respectively

$$\frac{\partial U'D'}{\partial t'} + \beta\left[\frac{\partial U'^2 D'}{\partial x'} + \frac{\partial U'V'D'}{\partial y'}\right] + \frac{1}{F_r^2} D' \frac{\partial \zeta'}{\partial x'} AU'|U'| - \left[\frac{\partial}{\partial x'} 2R_b U'D'^2 \frac{\partial U'}{\partial x'} + \frac{\partial}{\partial y'} R_b U'D'^2\left(\frac{\partial U'}{\partial y'} + \frac{\partial V'}{\partial x'}\right)\right] = 0 \tag{10}$$

$$\frac{\partial \phi'D'}{\partial t'} + \frac{\partial \phi'U'D'}{\partial x'} + \frac{\partial \phi'V'D'}{\partial y'} = R_d\left[\frac{\partial}{\partial x'}\left(D'D'_{xx}\frac{\partial \phi'}{\partial x'} + D'_{xy}\frac{\partial \phi'}{\partial y'}\right) + \frac{\partial}{\partial y'}\left(D'D'_{yx}\frac{\partial \phi'}{\partial x'} + D'D'_{yy}\frac{\partial \phi'}{\partial y'}\right)\right] \tag{11}$$

the non-dimensional variables being defined as

$$U' = U/U_0, \quad V' = V/U_0, \quad D' = D/Z, \quad \zeta' = \zeta/Z,$$
$$t' = (U_0/L)t, \quad x' = X/L, \quad y' = y/L, \quad \phi' = \phi/\phi_0$$

where L, U_0, Z and ϕ_0 are representative values in the harbour for a horizontal length, a velocity, a vertical length and a concentration, respectively; F_r is the

Table 3. Model : prototype scaling ratios for the non-dimensional scaling parameters

Scaling parameter	Model : prototype	
Horizontal scale (L)	1 : 400	1 : 200
Vertical scale (Z)	1 : 40	1 : 40
Distortion ratio	10 : 1	5 : 1
$F_r(=U_0/\sqrt{(gZ)})$	1 : 1	1 : 1
Velocity scale (U_0)	1 : 6·32	1 : 6·32
Time scale (L/U_0)	1 : 63·3	1 : 31·7
$\lambda(=C_f L/Z)$	~1 : 10	~1 : 5
R_b ($=C_e Z/L$)	~10 : 1	~5 : 1
R_d ($=C_d Z/L$)	~10 : 1	~5 : 1

Froude law scaling parameter ($=U_0/\sqrt{(gZ)}$); λ is the bed friction scaling parameter ($=C_f L/Z$); R_b is the bed-generated turbulence scaling parameter ($=\sqrt{(g)}Z/LC$); and R_d is the dispersion–diffusion scaling parameter ($=R_b$).

17. For the Froude law scaling relationship existing between the physical model and the prototype for dynamic similarity, the model : prototype ratios for the various non-dimensional scaling parameters, for the standard prototype mean depth, were as given in Table 3. From these results, it can be seen that the physical model underestimates the magnitude of frictional dissipation by a factor of about 10 and 5 for the small and large harbour, respectively; it overestimates the rate of transfer by bed-generated turbulence by a factor of about 10 and 5; and it overestimates the dispersion process by a similar factor of about 10 and 5.

18. In a similar manner the effects of a sloping bed on the tidal exchange in harbours can be predicted by considering the vorticity transport equation expressed in the form[3]

$$\frac{\partial \omega}{\partial t}+\frac{\partial U\omega}{\partial x}+\frac{\partial V\omega}{\partial y}=-\left[\frac{\partial}{\partial y}\left(\frac{\tau_{bx}}{\rho D}\right)-\frac{\partial}{\partial x}\left(\frac{\tau_{by}}{\rho D}\right)\right]+\left[\frac{\partial}{\partial y}\left(\frac{1}{\rho D}\frac{\partial D\tau_{xy}}{\partial y}\right)-\frac{\partial}{\partial x}\left(\frac{1}{\rho D}\frac{\partial D\tau_{yx}}{\partial x}\right)\right] \tag{12}$$

where ω is the depth-averaged vorticity, defined as $(\partial U/\partial y-\partial V/\partial x)$.

19. For the bottom friction term expressed in the form of a quadratic friction law as given by equation (6), and assuming C_f to be a constant, the corresponding term on the right-hand side of equation (12) can be expressed as

$$-\left[\frac{\partial}{\partial y}\left(\frac{\tau_{bx}}{\rho D}\right)-\frac{\partial}{\partial x}\left(\frac{\tau_{by}}{\rho D}\right)\right]=-\frac{C_f}{D}\left[\underbrace{|U|\omega}_{(i)}-\underbrace{\left(V\frac{\partial|U|}{\partial x}-U\frac{\partial|U|}{\partial y}\right)}_{(ii)}-\frac{|U|}{D}\underbrace{\left(U\frac{\partial D}{\partial y}-V\frac{\partial D}{\partial x}\right)}_{(iii)}\right] \tag{13}$$

where the terms (*i*), (*ii*) and (*iii*) refer to bottom friction dissipation, quadratic friction and bathymetric production, respectively.[7] In estimating the total vorticity at a point, contributions will arise from all three terms given in equation (13), with

the shear stress gradients in equation (12) small in comparison. However, for uniform bed slopes of either $dD/dx < 0$ or $dD/dy > 0$, the bathymetric production term will generally be positive for flood tide flows (with U/D and V/D being generally greater than 0), leading to increased vorticity and lateral velocity gradients, and hence, via three-dimensional effects, increased mixing and exchange. Thus, such an analysis of the vorcity transport equation indicates an increased exchange coefficients for negative and positive uniform bed slopes in the x and y directions, respectively.

Experimental results

20. In the first series of model tests undertaken, the mean depth was varied in both the 1 : 400 and the 1 : 200 model harbours, with the equivalent prototype depths being 4·5, 6·0, 7·0, 8·0 and 9·0 m, respectively. With the tidal range kept constant in both models, the corresponding model depths were 112·5, 150·0, 175·0, 200·0 and 225·0 mm, respectively, for a vertical scale ratio of 1 : 40 and distortion ratios of 10 : 1 and 5 : 1 for the small and large harbours, respectively. In these tests only dye concentration measurements were undertaken, as outlined in the preceding section, with the corresponding results illustrated in Fig. 3. As can be seen from the results, the exchange coefficient decreased almost linearly with increasing depth for both scale model harbours, with the smaller 1 : 400 scale model exhibiting slightly higher exchange ratios. This result is consistent with the scaling ratios given in Table 3, which indicate increased bed-generated turbulence and dispersion–diffusion in the smaller harbour model. In accounting for this physically, the clear water flood tide jet was observed to circumnavigate the harbour, with much of the incoming flood tide fluid being exhausted on the subsequent ebb tide. By increasing the relative effects of dispersion and diffusion with increased distortion, more of the relatively high concentration dye within the basin diffused across into the clear tidal jet to be exhausted on the subsequent ebb tide.

21. The main series of tests involved determining the velocity profiles along the axes AOC and BOD (Fig. 1) and the exchange characteristics for three different vertical scaling ratios, namely 1 : 33, 1 : 40 and 1 : 64, and for the two different

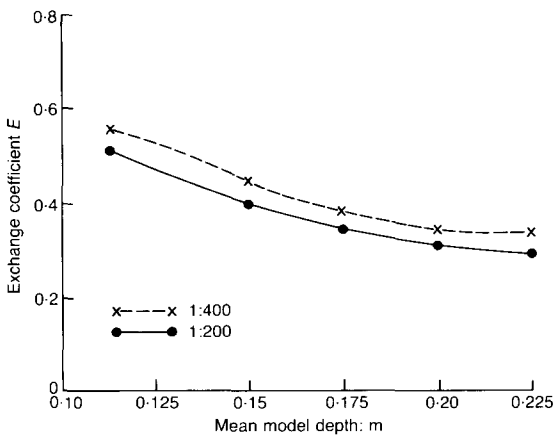

Fig. 3. Variation of exchange coefficient with depth for two horizontal scaling ratios

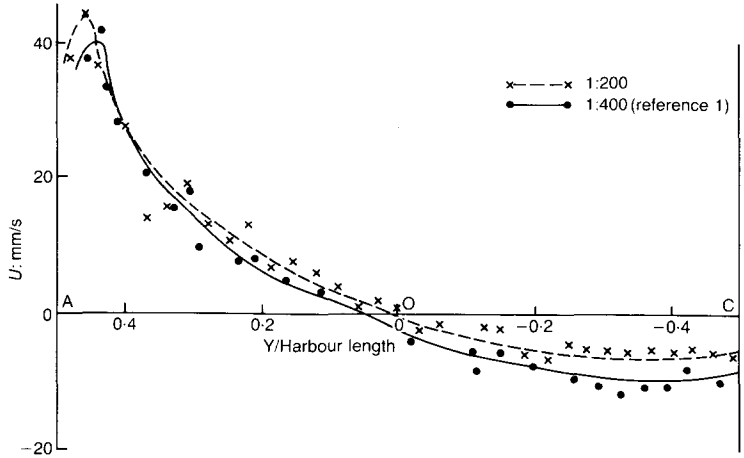

Fig. 4. Measured velocity profiles along the AOC axis at mean water flood tide for a 1 : 40 vertical scale and a flat bed

harbour sizes (i.e. for the 1 : 400 and 1 : 200 model horizontal scales), both with horizontal and uniformly sloping beds. As mentioned previously, the results were obtained to provide data for numerical model development and calibration, and to investigate the influence of scaling, distortion and bed slopes on the velocity profiles, and, in particular, the exchange characteristics of the idealized model harbours. A typical set of normalized velocities is illustrated in Figs 4 and 5 along the AOC axis, for both flood and ebb tides and for a distortion ratio of 10 : 1. Results are shown for the two horizontal scales of 1 : 200 and 1 : 400 and for a flat bed only.[1] Likewise, a similar set of results was obtained along the BOD axis and for the other vertical scales and distortion ratios considered. A typical set of numerical values is shown in Table 4.

22. To check the consistency of the float measuring technique used in the current study, measurements for the 10 : 1 distortion ratio were first compared

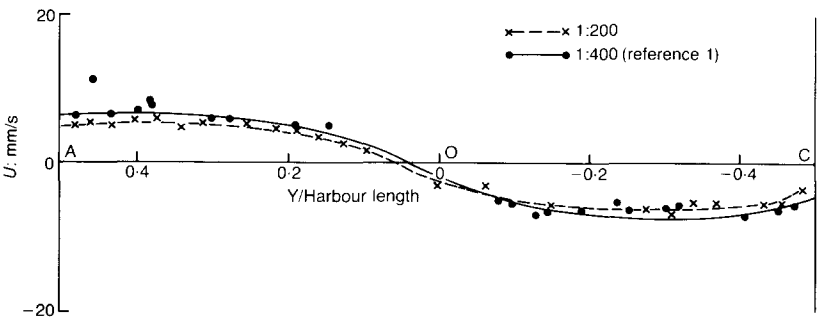

Fig. 5. Measured velocity profiles along the AOC axis at mean water ebb tide for a 1 : 40 vertical scale and a flat bed

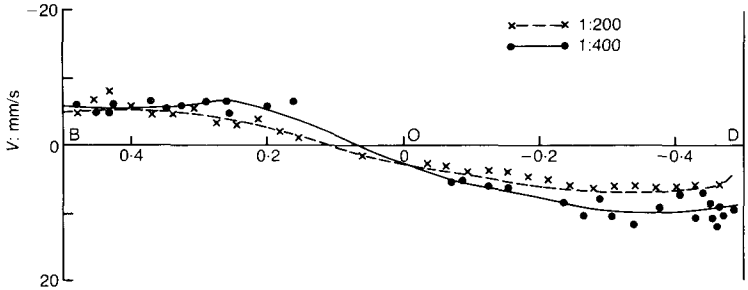

Fig. 6. Measured velocity profiles along the BOD axis at mean water ebb tide for a 10 : 1 distortion ratio

with those previously measured in reference 1. The corresponding results were found to give close repeatability, and Nece's results for the 1 : 400 model have been used for comparative purposes in the current study.

23. In comparing the present 1 : 200 model results with those previously recorded,[1] the disparities between the results in both sets are generally consistent, and the differences between the velocity profiles are in line with the implications of distortion highlighted in Table 3. Thus the comparisons show that the generally greater velocities in the 1 : 400 model are to be expected on account of decreased bed friction effects, with increased bed-generated turbulence effects of second-order importance relative to frictional dissipation.

24. The local and gross exchange coefficients were evaluated firstly for a horizontal bed and compared for three different vertical scales (i.e. 1 : 33, 1 : 40 and 1 : 64) and for each model horizontal scale (i.e. 1 : 400 and 1 : 200). The corresponding variations in the exchange coefficient with the scale ratios are given in Table 5, with the results indicating that in all but one case (a distortion ratio of 6 : 1), the exchange coefficient was reduced for increasing vertical scales, or reduced distortion ratios. This general result was again consistent with the interpretation of the non-dimensionalized form of the advective–diffusion equation. As the distortion ratio was increased, so too were the dispersion and diffusion effects, thereby giving increased dye mixing with the incoming clear water jet. As before, this jet then circumnavigated the harbour, thereby exhausting a higher dye concentration on the ebb tide for a greater distortion ratio. Hence the results of this study indicated that distorted hydraulic models generally lead to an overestimation of the gross exchange characteristics for square harbours with a tide-induced recirculating flow. The gradual effect of the circumnavigating jet of clear water tending to exhaust a higher dye concentration for greater distortion ratios on the ebb tide is also confirmed by the local exchange coefficients shown in Fig. 7, and with similar distributions being obtained for the other distortion ratios. As can be seen from these local exchange distributions, the higher exchange values generally occur around the perimeter points, with the exchange coefficients tending to be reduced continuously towards the centre of the harbour. Bearing in mind that a higher exchange coefficient indicates a reduced dye concentration, these results were consistent with visual observations, in that for a flat bed the highest dye concentration was observed to occur at, or near to, the eddy centre.

Table 4. Measured velocities for 1 : 200 scale model with 5 : 1 distortion ratio: (a) axis AOC; (b) axis BOD

Y : mm	U(flood : mm s^{-1})	U_f/U_0	U(ebb) : mm s^{-1}	U_e/U_0	X : mm	V(flood) : mm s^{-1}	V_f/U_0	V(ebb) : mm s^{-1}	V_e/U_0
+1040	+37·6	+1·31	+5·1	+0·18	+1040	−16·5	−0·57	−5·3	−0·18
1000	+43·9	+1·53	+5·3	+0·18	1000	−25·2	−0·88	−6·7	−0·23
933	+35·4	+1·23	+5·1	+0·18	933	−20·4	−0·71	−8·2	−0·29
867	+27·2	+0·94	+5·8	+0·18	867	−19·1	−0·67	−5·5	−0·19
800	+14·2	+0·49	+6·0	+0·20	800	−14·3	−0·50	−4·5	−0·16
733	+15·8	+0·54	+4·8	+0·21	733	−13·3	−0·46	−4·7	−0·16
667	+18·9	+0·66	+5·1	+0·17	667	−10·9	−0·40	−5·7	−0·20
600	+13·1	+0·46	+5·8	+0·18	600	−10·1	−0·35	−3·4	−0·12
533	+10·8	+0·38	+5·1	+0·20	533	−10·7	−0·37	−3·4	−0·12
467	+13·5	+0·47	+4·7	+0·18	467	−6·7	−0·23	−3·8	−0·13
400	+6·8	+0·24	+4·7	+0·16	400	−7·4	−0·26	−2·1	−0·07
333	+7·6	+0·26	+3·8	+0·16	333	−5·7	−0·20	−1·3	−0·05
267	+6·1	+0·21	+2·8	+0·13	267	−2·3	−0·08	−2·1	−0·07
200	+3·9	+0·13	+1·8	+0·10	200	−1·6	−0·06	−1·5	−0·05
133	+1·0	+0·03	+0·6	+0·06	133	−1·1	−0·04	+1·5	+0·05
67	+4·9	+0·17	−0·4	+0·02	67	−1·7	−0·06	+1·2	+0·04
0	+0·9	+0·03	−2·9	−0·01	0	+2·0	+0·07	+0·7	+0·02
−67	−2·2	−0·07	−2·9	−0·10	−67	+2·0	+0·07	+2·0	+0·07
−133	−2·1	−0·07	−2·8	−0·10	−133	+3·1	+0·11	+2·0	+0·07
−200	−1·3	−0·05	−0·8	−0·10	−200	+4·0	+0·14	+2·4	+0·08
−267	−1·1	−0·04	−0·9	−0·03	−267	+4·6	+0·16	+2·9	+0·10
−333	−1·8	−0·06	−5·1	−0·03	−333	+3·8	+0·13	+2·3	+0·08
−400	−5·8	−0·21	−1·9	−0·18	−400	+5·8	+0·20	+2·5	+0·09
−467	−6·2	−0·22	−2·0	−0·07	−467	+5·7	+0·20	+3·6	+0·13
−533	−4·0	−0·14	−1·5	−0·07	−533	+6·0	+0·21	+5·3	+0·18
−600	−4·4	−0·15	−5·9	−0·05	−600	+6·3	+0·22	+6·4	+0·22
−667	−5·3	−0·18	−5·8	−0·21	−667	+7·3	+0·25	+5·9	+0·21
−733	−5·3	−0·18	−4·8	−0·20	−733	+5·5	+0·19	+4·6	+0·16
−800	−4·9	−0·17	−4·6	−0·17	−800	+7·0	+0·24	+6·1	+0·21
−867	−5·6	−0·19	−2·3	−0·16	−867	+5·1	+0·18	+5·8	+0·20
−933	−5·0	−0·17	−4·6	−0·08	−933	+5·6	+0·20	+5·7	+0·20
−1000	−5·9	−0·21	−4·6	−0·16	−1000	+5·1	+0·18	+5·6	+0·20
−1040	−6·0	−0·21	−3·1	−0·11	−1040	+4·9	+0·17	+4·0	+0·14
		(*a*)					(*b*)		

Table 5. Variation of gross exchange coefficient with vertical and horizontal model scales for a horizontal bed

	Verticle scale		
Horizontal scale	1 : 33	1 : 40	1 : 64
1 : 400 (distortion ratio)	0·449 (12 : 1)	0·439 (10 : 1)	0·434 (6·25 : 1)
1 : 200 (distortion ratio)	0·427 (6 : 1)	0·424 (5 : 1)	0·391 (3·125 : 1)

25. Finally, a series of tests was undertaken for uniformly sloping bed inclinations of 10 and 5%, for the 1 : 400 and 1 : 200 horizontal scale model harbours, respectively. The tests were carried out for inclinations in both the x and y directions, with the entrance depth and velocity (equation (2)) being the same as those for the flat bed at the same tidal phase. Thus the corresponding bed slopes considered were $-0{\cdot}1$ and $-0{\cdot}05$ for dD/dx and 0·1 and 0·05 for dD/dy.

26. The corresponding gross exchange coefficients are given in Table 6, with the main observation being that, with the exception of the 6 : 1 distortion ratio, the gross exchange coefficients obtained for a sloping bed were typically found to be 8–50% higher than those measured for a flat bed. This general observation is again consistent with the predicted analysis of the vorticity equation, wherein negative and positive bed inclinations in the x and y directions, respectively, indicated increased vorticity generation through the bottom friction term. Further analysis of Table 6 indicates that the exchange coefficient is greater for all distortion ratios when the inclination is normal (i.e. x direction slope) rather than parallel (y direction slope) to the entrance plane. A typical local exchange distribution is given in Fig. 8 for a sloping bed (i.e. $dD/dy > 0$), and comparison with Fig. 7 indicates a significantly increased spatial variation in the exchange coefficient, with higher values at the rear end of the harbour for the sloping bed.

27. Similar comparisons were also undertaken of the velocity profiles across the AOC and BOD axes for the inclined and horizontal bed. The resulting com-

Table 6. Variation of gross exchange coefficients with distortion ratio for bed slopes in the x and y directions

Distortion ratio	Bed slope		
	$dD/dx < 0$ $dD/dy = 0$	$dD/dx = 0$ $dD/dy > 0$	$dD/dx = 0$ $dD/dy = 0$
12 : 1	0·487	0·486	0·449
10 : 1	0·510	0·479	0·439
6·25 : 1	0·551	0·476	0·434
6 : 1	0·456	0·441	0·427
5 : 1	0·463	0·436	0·424
3·125 : 1	0·551	0·489	0·391

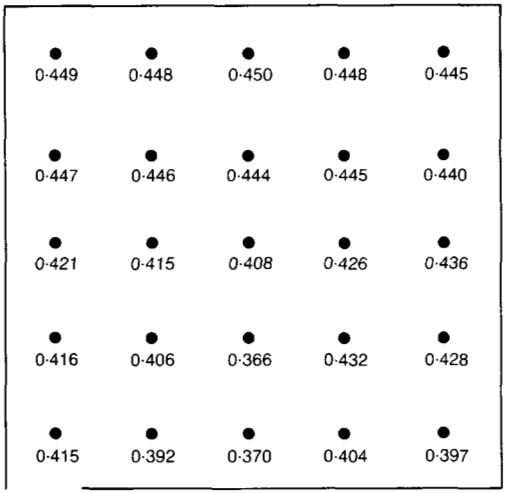

Fig. 7. Measured exchange coefficient for a distortion ratio of 5 : 1 and a flat bed

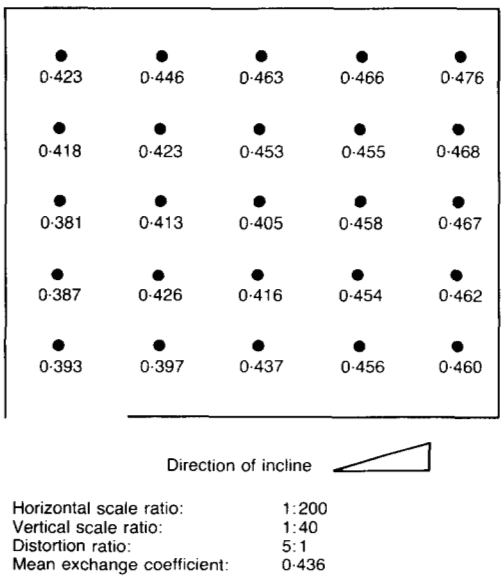

Fig. 8. Measured exchange coefficient for a distortion ratio of 5 : 1 and an inclined bed along entance plane

parisons indicated little difference in the ebb tide velocity profiles for the various slope and distortion ratios considered. However, for the flood tide comparisons, the U velocity magnitudes were generally larger between A and O for both bed slopes when compared with those measured for the horizontal bed, whereas the corresponding velocity magnitudes were smaller for both inclination directions between B and O. For the velocity components along the OC and OD axes there were only minor differences between the measured values for the inclined and horizontal beds.

Conclusions

28. The Paper has described the results of a series of laboratory model tests, aimed primarily at obtaining laboratory data to verify and enhance the predictive capability of refined numerical models.

29. In addition to provision of some of the data, attempts have also been made to investigate the effects of variations in the mean depth, the horizontal and vertical model scales and bed slopes on the velocity profiles and the tidal exchange coefficients for two square model harbours. The corresponding results showed that the tidal exchange coefficient reduced strongly with increasing depth, giving rise to enhanced flushing efficiencies in shallower basins. Furthermore, the comparative exchange coefficients were found to be less for the larger hydraulic model, confirming the findings of a scaling analysis which indicated higher dispersion–diffusion effects for increased depth.

30. In comparing non-dimensional velocity profiles for the 1 : 400 and 1 : 200 horizontal model scale harbours, there was little difference between the two profiles. However, the consistent difference showed that the velocity magnitudes were generally slightly larger for the 1 : 400 scale model, as predicted for the reduced bed friction effects for higher distortion ratios.

31. For the gross exchange coefficient comparisons for various horizontal and vertical length scales, the results showed that for a flat bed the gross exchange coefficients were reduced for increasing vertical scale ratios and reduced distortion ratios. This was accounted for by noting that enhanced dispersion–diffusion occurred for higher distortion ratios, which led to greater dye mixing with the flood tide circumnavigating clear water jet, which in turn led to the exhaust of more dye on the subsequent ebb tide.

32. Local exchange coefficient distributions also confirmed the influence of the circumnavigating flood tide jet, with the local exchange values generally increasing radially outwards from the harbour centre. Bearing in mind that a higher exchange coefficient indicates higher flushing, this result indicates that the maximum flushing occurs around the harbour or eddy perimeter, and with the highest dye concentrating at or near to the eddy centre.

33. For the gross exchange coefficient comparisons with sloping beds, the results showed that the exchange coefficients were generally higher than those measured with a flat bed, with higher local exchange values being recorded at the rearmost part of the harbour. This general observation was consistent with an analysis of the vorticity transport equation, wherein higher velocity gradients were predicted nearer to the centre of the tidal eddy as a result of inclined beds. The corresponding velocity comparisons also showed higher jet velocities along the positive axes, with the origin located at the harbour centre. Thus the engineering implications of this result are that the local exchange, and hence absolute concen-

tration levels, can be reduced at the rearmost part of a square harbour with a tidal eddy if the bed is inclined upwards and away from the harbour entrance.

Acknowledgements

34. The work described here was undertaken in the hydraulics laboratory at the University of Bradford. The Authors thank Dr B. Chapman and Mr R. C. Boase for design of the tidal basin, and in particular Mr A. Daren (Hydraulics Technician) for his assistance. The Authors also thank Professor R. E. Nece for his support and encouragement during his sabbatical year at Bradford University.

35. The Authors are grateful to the British Council for funding the second Author's period of leave at Bradford University, and to Tongji University, Shanghai, and Professor Gu Guowei (Head of the Department of Environmental Engineering) for their support and interest.

36. The Authors are also grateful to Scan Technologies Ltd, Ilkley, for donation of a sophisticated acoustic water level recorder for this research programme.

References

1. NECE R. E. Tidal current measurements in a laboratory harbour. *J. Hydraul. Engng Div. Am. Soc. Civ. Engrs*, submitted for publication.
2. NECE R. E. and FALCONER R. A. (FALCONER R. A. *et al.* (eds)). Modelling of tide induced depth averaged velocity distributions in a square harbour. *Hydraulic and environmental modelling of coastal, estuarine and river water*. Gower Publishing, Aldershot, 1989, 56–66.
3. FALCONER R. A. and MARDAPITTA-HADJIPANDELI L. Bathymetric and shear stress effects on an island's wake: a computational model study. *Coastal Engng*, 1987, **11**, 57–86.
4. MARDAPITTA-HADJIPANDELI L. and FALCONER R. A. Some observations on nested modelling of flow and solute transport in rectangular harbours. *Proc. Instn Civ. Engrs*, Part 2, 1990, **89**, Mar., 15–38.
5. NECE R. E. Physical modelling of tidal exchange in small-boat harbours. *Proc. Int. Conf. on Numerical and Hydraulic Modelling of Ports and Harbours*, Birmingham, April 1985, 33–41.
6. NECE R. E. and RICHEY E. P. Application of physical tidal models in harbour and marina design. *Proc. Symposium on Modelling Techniques*, San Francisco, 1975, **1**, 783–801.
7. PINGREE R. D. and MADDOCK L. The effects of bottom friction on the Earth's rotation on an island's wake. *J. Mar. Biol. Ass.*, 1980, **60**, 499–508.